Gas- and Water-phase PAHs Emitted from a Single Hydrogen-Oxygen PEM Fuel Cell

Kuo-Lin Huang[1],*, Tsung-Hsuan Tsai[1], Shui-Jen Chen[1], How-Ran Chen[1], Yi-Ming Kuo[2], Jen-Hsiung Tsai [1]

[1]*Department of Environmental Engineering and Science, National Pingtung University of Science and Technology, Neipu, Pingtung 91201, Taiwan*

[2] *Department of Safety Health and Environmental Engineering, Chung Hwa University of Medical Technology, Tainan City 71703, Taiwan*

Abstract

This study focuses on the comparison between gas- and water-phase polycyclic aromatic hydrocarbons (PAHs) emitted from a single hydrogen-oxygen proton exchange membrane (PEM) fuel cell (FC) under different flowrates and temperatures. The results show that among 21 PAHs, the most and least dominant species were Nap and BeP, respectively. At 65°C, the concentrations of individual gas- and water-phase PAHs decreased with increasing flowrate, and the PAH concentrations were lower at anode than at cathode. The concentrations of gas-phase Total-PAHs or Total-BaP_{eq} were slightly lower at 65°C than at 90°C, but an opposite trend was observed for water-phase ones. Temperature influenced more on water-phase than on gas-phase PAH concentration profiles, and the gas- and water-phase PAHs had different concentration profiles. The performance of membrane-electrode assembly (MEA) decreased with increasing flowrate or temperature. The emission factor (EF) sum (anode + cathode) for gas- or water-phase Total-PAHs increased with increasing flowrate. This tendency is also true for gas-phase Total-PAHs EFs but not for water-phase ones when raising temperature from 65°C to 90°C. At 65°C and 52/35 sccm, the EF sums of water-phase Total-PAHs and Total-BaP_{eq} were 2.18±0.04 and 0.09±0.00 μg g-MEA^{-1}, respectively, smaller than those of gas-phase ones (3.02±0.09 and 0.12±0.00 μg g-MEA^{-1}, respectively). More environmental concern should be paid to the emitted gas-phase PAHs than water-phase ones because the anode and cathode effluents should be recycled and reused during PEMFC operation.

Keywords: Polycyclic Aromatic Hydrocarbon; Proton Exchange Membrane Fuel Cell; Emission Factor; Gas-phase PAH; Water-phase PAH.

* Corresponding author. Tel.: +886-8-7703202 ext. 7092; Fax: +886-8-7740256.
E-mail: huangkL@mail.npust.edu.tw

INTRODUCTION

Hydrogen-oxygen proton exchange membrane fuel cells (PEMFCs), regarded as a zero-emission green power generators, are promising alternative power sources for stationary and mobile applications (Wang *et al.*, 2006). The key advantages of PEMFCs are high energy conversion efficiencies, quick start-up, and zero by-product emissions (Tenson and Baby, 2017). An H_2-O_2 PEMFC has the main components of membrane-electrode assembly (MEA), gas-diffusion layer (GDL), and bipolar/end plate (Huang *et al.*, 2006; Lai *et al.*, 2012; Tenson and Baby, 2017). It is common that a PEM is symmetrically sandwiched by anode and cathode to prepare the MEA; moreover, the electrodes usually contain precious metal catalysts (e.g., Pt) (Huang *et al.*, 2006; Lai *et al.*, 2012), Pt-based alloys (Zhang *et al.*, 2017), or non-platinum group metals (Reshetenko, *et al.*, 2016) supported by carbon materials (e.g., carbon black, fiber, and nanotube) which are also used for the fabrication of bipolar/end plates and GDLs (e.g., carbon paper or cloth) (Tran *et al.*, 2015; Zeis, 2015; Lee and Lee, 2016).

Extensive study has concentrated on accelerating the sluggish kinetics of cathode catalyst, minimizing overall Pt content, and increasing membrane proton conductivity for PEMFCs (Scofield *et al.*, 2015; Tenson and Baby, 2017). Furthermore, hydrogen powered fuel cell electric vehicles are classed as ultra-low emission vehicles when supposing water vapor as the only emission substance in exhaust; therefore, the use of hydrogen powered fuel cell electric vehicles can reduce the emissions of pollutants (which degrade local air quality) and carbon dioxide. However, little attention has been paid to the emission of polycyclic aromatic hydrocarbons (PAHs) from PEMFCs

(Huang *et al.*, 2015; Huang *et al.*, 2016),

PAHs have long been concerned for their adverse impacts on health and the environment (Tiwari *et al.*, 2015; Kavouras *et al.*, 2015; Pongpiachan, 2016; Li *et al.*, 2017). PAHs can be generated from pyrogenic, petrogenic, biogenic, or diagenetic (indoor/outdoor) sources (Stogiannidis and Laane, 2015; Kavouras *et al.*, 2015; Mwangi *et al.*, 2015; Zhang *et al.*, 2016; Li *et al.*, 2017; Fan *et al.*, 2017; Lai *et al.*, 2017). In our previous works, we reported the emissions of 21 PAHs from a H_2-O_2 PEMFC (installed by a lab-prepared MEA with the same Pt loading of 0.5 mg cm^{-1} on anode and cathode) (Huang *et al.*, 2015) and effect of operating conditions on PAHs emission from the PEMFC (Huang *et al.*, 2016). In this study, we explored the emissions, concentration profiles, and emission factors of gas- vs. water-phase PAHs from the PEMFC under different flowrates and temperatures.

MATERIALS AND METHODS

Membrane-Electrode Assembly (MEA) and Fuel Cell Emission Test

The membrane-electrode assemblies (MEAs) tested in this study were all E-TEK commercial MEAs purchased from Micro Power Fuel Cell Co., Ltd. These MEAs had the same catalyst loading in both anode and cathode (0.4 mg-Pt cm^{-2}) which were separated with a proton exchange membrane (Nafion-117). An MEA commonly consists of a proton exchange membrane (solid electrolyte), two dispersed catalyst layers, and two gas diffusion layers (GDL). The structure of MEA was addressed in our earlier papers (Huang *et al.*, 2006; Lai *et al.*, 2012; Huang *et al.*, 2015; Huang *et al.*, 2016).

The single H_2-O_2 PEMFC used in PAH emission tests had an MEA symmetrically sandwiched by Telfon gaskets, carbon (graphite) blocks (with gas flow channel), and copper current collectors. The single cell was installed on a standard fuel cell test

station that worked at 65°C or 90 °C (80°C and 70°C for the anode and cathode humidifiers, respectively) and 0.6 V for 48 h for PAH collection under different anode hydrogen and cathode oxygen flow rates which were regulated by two mass flow controllers. The details of sampling system connected to the single cell and PAH collection were provided in our previous works (Huang *et al.*, 2015; Huang *et al.*, 2016). For comparison, the PAH emissions from the single PEMFC were also tested at various anode/cathode flowrates of 30/18, 100/100, and 200/200 sccm. It is almost impossible to form PAHs under the operating conditions of this study because it is an electrochemical process and the only "fuel" was hydrogen, so the PAHs collected from the anode/cathode emission gases and effluents were mainly from the desorption of PAHs which originally absorbed on the carbon materials of MEA in the fuel cell during operation (Huang *et al.*, 2015; Huang *et al.*, 2016).

PAH Sampling, Analysis, and Quality Control

In this study, the PAH sampling system, connected to the PEMFC, simultaneously collected PAHs from the anode and cathode emission ports. For each sampling, a glass water collector was used to collect the cell effluent containing water-phase PAHs; the water collector was serially connected with a glass cartridge (packed with XAD-16 resin granules and supported by a polyurethane foam (PUF) plug) for the collection of gas-phase PAHs (Fig. 1). Triplicate PAH samplings (n = 3) were conducted in each experiment. After PAH collection, cell polarization tests were performed at different anode/cathode flowrates or cell temperatures.

We measured 21 PAHs: Naphthalene (Nap), Acenaphthylene (AcPy), Acenaphthene (Acp), Fluorene (Flu), Phenanthrene (PA), Anthracene (Ant), Fluoranthene (FL), Pyrene (Pyr), Benzo(a)anthracene (BaA), Chrysene (CHR), Cyclopenta(c,d)pyrene (CYC), Benzo(b)fluoranthene (BbF), Benzo(k)fluoranthene

(BkF), Benzo(e)pyrene (BeP), Benzo(a)pyrene (BaP), Perylene (PER), Indeno(1,2,3,-cd)pyrene (IND), Dibenzo(a,h)anthrance (DBA), Benzo(b)chrycene (BbC), Benzo(ghi)perylene (BghiP) and Coronene (COR). The 21 PAH species were classified into three categories: low molecular weight (LMW-PAHs, 2-/3-ring PAHs: NaP, AcPy, AcP, Flu, Ant, and PA), middle molecular weight (MMW-PAHs, 4-ring PAHs: FL, Pyr, BaA, and CHR), and high molecular weight (HMW-PAHs, 5-/6-/7-ring PAHs: CYC, BbF, BkF, BeP, BaP, PER, DBA, BbC, IND, BghiP, and COR). The Total-PAHs concentration was obtained from the sum of the concentrations of 21 PAH species.

The details of PAHs extraction by Soxhlet extraction method, the identification/quantification of PAHs (with blank correction) by gas chromatograph/mass spectrometry (GC/MS), and the quality assurance (QA)/quality control (QC) procedures for PAHs GC/MS analysis were stated elsewhere (Huang *et al.*, 2015). The correlation coefficients of the calibration curves were 0.995–0.999. Ten consecutive injections of a PAH 610-M standard yielded an average relative standard deviation (RSD) of the GC/MS integration area of 3.0% with a range of 0.8–5.1%. The total recovery efficiencies of PAHs from seven consecutive injections ranged from 74 to 110%, while the average recoveries of the five internal standards were 85–93% across seven consecutive injections.

The coefficients of variation for repeat injections of the standard solution (containing PAH Mixture-610 M (16 PAHs) and five Merck PAH standards) were all less than 5% for all of the analyzed PAHs, whereas those obtained by replicate analysis were 2–10%. Analyses of serial dilutions of PAH standards revealed the limits of detection (LODs) of GC/MS to be between 0.010 and 0.474 ng for the 21 PAH compounds. The limit of quantification (LOQ) was defined as the LOD divided by the sampling volume. The LOQ values of the 21 PAH compounds for cell effluent

and emission gas were 0.102–2.470 ng L^{-1} and 0.076–0.175 ng Nm^{-3}, respectively.

RESULTS AND DISCUSSION

Effect of Flowrate on Gas-phase PAHs Emission

For the tests of PEMFC PAH emissions at different flowrates, the anode/cathode flowrates of 52/35 sccm represents 1.5 and 2 times of the stoichiometric requirements for the anode and cathode feeding gases, respectively (Huang *et al.*, 2006; Lai *et al.*, 2012; Huang *et al.*, 2015; Huang *et al.*, 2016). Fig. 2 shows the anode and cathode concentration profiles of gas-phase 21 PAHs collected from the exhaust of fuel cell operated at 65°C and different flowrates. At anode/cathode flowrates of 52/35 sccm, the concentrations of PAHs in anode and cathode emission gas ranged from not detectable (ND) (BeP) to 2.961±0.005 (Nap) and ND (BeP) to 4.115±0.005 (Nap) μg Nm^{-3}, respectively (Fig. 2(a)), while most of the other species had concentrations of 0.200–0.800 μg Nm^{-3}. The same PAH species showed a higher concentration in the cathode emission gas than in the anode one. A similar trend was also found at the lower anode/cathode flowrates of 30/18 sccm (Fig. 2(b)). This phenomenon is mainly attributed to the fact that the sampling volume was greater at anode than at cathode but both electrode had similar or slightly different PAH mass emission, regardless of the difference in operation between anode and cathode.

The operating potential of anode was <1.23 V (theoretical) vs. standard hydrogen electrode (SHE), while that of cathode was ~ 0 V vs. SHE. Moreover, the main electrochemical reaction at anode is hydrogen oxidation which can be expressed as the following reaction:

$$H_2 \rightarrow 2H^+ + 2e^- \quad (1).$$

On the other hand, the principle electrochemical reaction at cathode is oxygen reduction, described by reaction 2:

$2H^+ + 2e^- + 1/2O_2 \rightarrow H_2O$ (2).

Nevertheless, the emission concentration of the same PAH species was lower at 30/18 sccm than at 52/35 sccm, because the former emitted much less PAH mass than the latter, although the sampling volume was lower at 30/18 sccm than at 52/35 sccm (see more discussion in the last section).

Dissimilarly, the concentration of individual PAH species decreased, when the gas flowrate increased from 52/35 to 100/100 sccm, except NaP (Fig. 2(c)); hence, the emission of Nap was more influenced by flowrate than those of the other PAH species. This result is majorly attributable to the higher sampling volume at the greater flowrate, although more PAH mass was present in the anode and cathode emission gases at the greater flowrate (see more discussion in the last section). In our earlier study, we also observed this phenomenon when using the same sampling volume at different flowrates (52/35 and 100/100 sccm) or different sampling volumes (or time periods: 12, 24, and 36 hr) at the same flowrate (52/35 sccm) (Huang *et al.*, 2016). When the gas flowrate further increased from 100/100 to 200/200 sccm, more PAHs desorption occurred and thus was collected in the anode or cathode emission gas (see more discussion in the last section) (Fig. 2(d)). Therefore, flowrate significantly influenced the desorption of PAHs from carbon black support during operation, despite the possible strong π-π interaction between PAHs and the graphitic structure of carbon materials (Kah *et al.*, 2011) and the fact that PAHs are relatively easier to adsorb on than to desorb from the surface of carbon blacks (Moninot, 2010).

Of all the 21 PAHs, NaP was the most predominant species at different flowrates while BeP was only detected at 200/200 sccm. Some PAH species such as Flu, CHR, BkF, BbC, and COR were comparably dominant as PA at 30/18, 52/35 and 100/100 sccm, but these compounds were significantly less dominant than PA at 200/200 sccm. Consequently, flowrate also affected the desorption of individual PAH species and

thus its dominance in the anode and cathode emission gases. This result is also probably associated with the electronegative functional groups of compounds, because aromatic compounds having strong electronegative functional groups generally form stronger bonds with the graphene surface of carbon materials (Ma and Uddin, 2013).

Effect of Flowrate on Water-phase PAHs Emission

For comparison, the water-phase PAHs emitted from anode and cathode gases were also collected under the same operating conditions used for gas-phase PAHs sampling. Like the trend of anode versus cathode PAH concentration comparison for gas-phase PAHs, the concentrations of individual PAHs were significantly greater in cathode effluent than in anode effluent (except BkF and BghiP) at 65^{o}C and different flowrates (Figs. 3(a)–(d)). Again, among the 21 PAHs, NaP had the highest concentration, followed by Flu, COR, PA, BbC, CHR, and FL, while BeP was not detected under all tested flowrates. However, the concentration difference between the highest (NaP) and the second highest was less for water-phase PAHs than for gas-phase PAHs. This result should be associated with the fact that the 21 PAHs have low water solubility. Roughly, the water solubility of PAHs decreases as the aromatic ring number increases; for example, the solubility data of Nap, Pyr, and BaP at 25^{o}C are 31.0, 0.132, and 0.0038 mg L^{-1}, respectively (ER Wiki, 2017). The NaP concentrations in anode effluents at 30/18, 52/35, 100/100, and 200/200 sccm were 1.759±0.057, 0.766±0.122, 0.419±0.053, and 0.220±0.028 μg L^{-1}, respectively, while the corresponding data in cathode effluents were 8.530±0.178, 3.871±0.253, 2.325±0.061, and 0.954±0.060 μg L^{-1}, respectively. BeP was not detectable (ND) in the anode and cathode effluents at all the tested flowrates.

It was also observed that the concentrations of individual water-phase PAHs were

smaller at anode/cathode flowrate = 52/35 sccm than at anode/cathode flowrate = 30/18 sccm, mainly because the collected water volume was greater at 52/35 sccm (Fig. 3(a)) than at 30/18 sccm (Fig. 3(b)), but their emitted PAH masses were comparable (see more discussion in the last section). For the same reason, the concentrations of individual PAHs were greater at 52/35 sccm than at 100/100 sccm (Fig. 3(c)). This tendency is also true when increasing the flowrate to 200/200 sccm (Fig. 3(d)).

Effect of Temperature on Gas- and Water-phase PAHs

Fig. 4(a) shows the concentration profiles of 21 individual PAHs in anode and cathode emission gases at 90^{o}C and 52/35 sccm. Again, the concentration of BeP was ND in anode and cathode emission gases. This result is also true in the anode and cathode effluents (Fig. 4(b)). In anode emission gas, the concentrations of individual PAHs ranged from 0.102±0.111 (DBA) to 3.055±0.358 (NaP) μg Nm^{-3}, excluding BeP; the corresponding values were from 0.152±0.001 (DBA) to 4.585±0.718 (NaP) μg Nm^{-3} in cathode emission gas. However, they ranged from 0.168±0.003 (DBA) to 0.557±0.106 (NaP) μg L^{-1} in anode effluent and from 0.192±0.001 (BghiP) to 2.856±0.205 (NaP) μg L^{-1} in cathode effluent. The concentrations of individual PAHs were also higher in the anode side than in the cathode side, except that of water-phase BkF at 90^{o}C. At 52/35 sccm, the concentrations of gas-phase PAHs were similar at both 65^{o}C (Fig. 2(a)) and 90^{o}C (Fig. 4(a)), while the water-phase PAH concentrations were greater at 65^{o}C (Fig. 3(a)) than at 90^{o}C (Fig. 4(b)), consistent with the fact that the water solubility of a PAH species was lower when the temperature is higher.

Comparison of Gas- and Water-phase PAH Emission Profiles

In this study, the concentrations of gas- and water-phase individual PAHs in

anode and cathode emission gases were normalized to those of Total-PAHs for the comparison of their emission profiles (fingerprints) which denoted the fraction of a PAH species (PAH_i, i = 1–21) using the following calculation:

Fraction (%) of PAH_i = 100×(concentration of PAH_i/concentration of Total-PAHs) (3).

For the anode emission under various flowrates or temperatures, the concentration profiles of gas-phase individual PAHs were similar (Fig. 5(a)). A similar trend was also observed for the gas-phase individual PAHs from cathode emission (Fig. 5(b)). Moreover, the concentration profiles of individual PAHs from anode and cathode emission gases were similar. Therefore, the flowrate or temperature in the tested ranges did not significantly influence the concentration profile of gas-phase individual PAHs. On the other hand, the concentration profiles of water-phase individual PAHs from anode effluent looked various in the sector from BkF to DBA at the lowest and highest feeding gas flowrates (30 and 200 sccm, respectively), although the profiles in the other sector were similar (Fig. 5(c)). This tendency was also observed for the PAH concentration profiles of cathode effluents in the sector from BaA to DBA; in addition to feeding gas flowrate, temperature (90^{o}C) also affected the pattern of profile (Fig. 5(d)). However, the PAH concentration profiles of cathode effluents were not similar to those of anode effluents in the sector from BaA to DBA. These findings might be related to the effect of feeding gas flowrate or temperature on the PAH water solubility, particularly for the PAHs with relatively low water solubility (BaA, CHR, BbF, BkF, PER, IND, and DBA) (ER Wiki, 2017). Moreover, the concentration profiles of water-phase PAHs were largely dissimilar to those of gas-phase PAHs. The partitioning of individual PAH species between gas and water phases should be responsible for this difference (Lee *et al.*, 2004).

Effect of Flowrate and Temperature on Gas-phase PAHs-associated BaP_{eq}

Emission

At 52/35 sccm, the concentrations of molecular-weight (MW) classified PAHs in anode and cathode emission gases varied with the order LMM- > HMM- > MMM-PAHs (4.421±0.038, 2.942±0.003, and 1.536±0.038 μg Nm^{-3}, respectively for anode (Fig. 6(a)) and 6.504±0.612, 4.442±0.061, and 2.236±0.120 μg Nm^{-3}, respectively for cathode (Fig. 6(b)). This phenomenon also existed at anode/cathode flowrate = 30/18, 100/100, and 200/200 sccm, except the HMM- > LMM- > MMM-PAHs at 18 sccm. This result is attributable to the more concentration variation for LMW-PAHs than for MMW- and HMW-PAHs (particularly Nap) during the operation at different anode/cathode flowrates. The Total-PAHs concentration decreased with the increase of flowrate in the range 52/35–200/200 sccm, chiefly due to the increase of sampling volume with increasing flowrate. This result is not consistent with our previous work using lab-prepared E-TEK MEAs (Huang *et al.*, 2016). However, the Total-PAHs concentration also decreased when the flowrate reduced from 52/35 (8.892±0.079 and 13.18±0.792 μg Nm^{-3} for anode and cathode, respectively) to 30/18 (6.834±0.452 and 10.37±0.395 μg Nm^{-3} for anode and cathode, respectively) sccm, mainly because of the less PAH mass emitted at the lower flowrate (see more discussion in the last section).

Fig. 6(c) presents that the concentrations of classified PAHs in anode and cathode emission gases also followed the order LMM- > HMM- > MMM-PAHs at 90^{o}C and anode/cathode = 52/35 sccm. However, the average LMM-PAHs concentration was greater at the anode side than at the cathode side, opposite to the observation of average HMM-PAHs concentrations at these two side. The concentrations of LMW-, MMW-, HMW-, and Total-PAHs were similar at both temperatures, so the emission of PAHs was more influenced by flowrate than by temperature. At 90^{o}C, the concentrations of anode LMW-, MMW-, HMW-, and

296 Total-PAHs were 4.984±0.381, 1.416±0.012, 2.980±0.035, and 9.380±0.429 μg Nm^{-3},
297 respectively, while the cathode ones were 7.409±0.764, 2.150±0.102, 4.426±0.077,
298 and 13.99±0.944 μg Nm^{-3}, respectively.

299 In this study, we calculated the benzo(a)pyrene (BaP)-equivalent carcinogenic
300 potency (BaP_{eq}) of a PAH species based on the product of its toxic equivalence factor
301 (TEF) and concentration (Nisbet and LaGoy, 1992). (Noted that BaP and DBA had the
302 highest TEF values (1) of all the 21-PAH.) The PAH-derived Total-BaP_{eq}
303 concentration decreased with increasing flowrate (30/18 (0.547±0.003/0.675±0.003
304 μg Nm^{-3}), 52/35 (0.365±0.001/0.546±0.004 μg Nm^{-3}), 100/100
305 (0.305±0.003/0.378±0.002 μg Nm^{-3}), and 200/200 (0.269±0.020/0.282±0.016 μg
306 Nm^{-3}) sccm) in anode and cathode emission gases (Figs. 6(a) and (b), respectively).
307 Nevertheless, The Total-BaP_{eq} concentration in anode or cathode gas only slightly
308 changed when raising temperature from 65°C to 90°C (0.365±0.001 and 0.542±0.003
309 μg Nm^{-3} for anode and cathode, respectively (Fig. 6(c))).

310

311 ***Effect of Flowrate and Temperature on Water-phase PAHs-associated BaP_{eq}***
312 ***Emission***

313 The concentrations of MW-classified PAHs at 52/35 sccm in anode effluent
314 were in the order HMM- > LMM- > MMM-PAHs (3.646±0.065, 2.956±0.214, and
315 1.655±0.010 μg L^{-1}, (Fig. 7(a)), but those in cathode effluent followed the order
316 LMM- > HMM- > MMM-PAHs (14.54±0.258, 12.81±0.109, and 8.195±0.037 μg L^{-1},
317 respectively (Fig. 7(b)). This phenomenon was also found at anode/cathode flowrate =
318 30/18, 100/100, and 200/200 sccm. Moreover, the MW-classified PAH concentrations
319 were significantly smaller in the anode effluent than in the cathode effluent regardless
320 of the difference in flowrate, mostly resulted from the observation that the water
321 volume collected from anode was lower than (approximately one-fifth) that collected

322 from cathode at each anode/cathode flowrate. For the same reason, both anode and
323 cathode effluents exhibited decreasing Total-PAHs concentration with increasing
324 flowrate, dissimilar to the observation for anode and cathode emission gases. As a
325 result, the Total-BaP_{eq} concentration also decreased with increasing flowrate (30/18
326 (0.593±0.001/1.086±0.002 μg L^{-1}), 52/35 (0.440±0.003/0.893±0.005 μg L^{-1}), 100/100
327 (0.393±0.004/0.775±0.008 μg L^{-1}), and 200/200 (0.386±0.004/0.819±0.004 μg L^{-1})
328 sccm) in anode and cathode effluents (except that in cathode effluent at 200/200 sccm
329 (Figs. 7(a) and (b), respectively).

330 At 90°C and anode/cathode = 52/35 sccm, similar to the trend for anode and
331 cathode emission gases at 65°C, the MW-classified PAH concentrations in anode
332 effluent varied with the order HMM- > LMM- > MMM-PAHs, while those in cathode
333 effluent followed the order LMM- > HMM- > MMM-PAHs (Fig. 7(c)). Additionally,
334 the classified PAH concentrations were also significantly smaller in the anode effluent
335 than in the cathode effluent. However, the concentrations of LMW-, MMW-, HMW-,
336 and Total-PAHs were higher at 65°C than at 90°C (anode: 2.655±0.100, 1.644±0.003,
337 3.641±0.053, and 7.940±0.149 μg L^{-1}, respectively; cathode: 13.48±0.086,
338 7.318±0.032 11.30±0.071, and 32.09±0.185 μg L^{-1}, respectively). The Total-BaP_{eq}
339 concentration in anode effluent was smaller at 65°C (0.440±0.003 μg L^{-1}) than at 90°C
340 (0.524±0.004 μg L^{-1}; however, this tendency was reversed for cathode effluent
341 (0.893±0.005 and 0.818±0.003 μg L^{-1} at 65°C and 90°C, respectively) (Fig. 7(c)).
342
343 ***Polarization Curves and Emission Factors***

344 According to the polarization (current-potential) curves shown in Fig. 8, the
345 performance of MEA installed in the PEMFC decreased when flowrate increased at
346 65°C. Furthermore, the MEA performance was even worse at 90°C, which had quick
347 potential drop at current density smaller than 100 mA cm^{-2}, probably because the

Nafion-117 membrane was drier to have lower conductivity at the higher temperature. However, the MEA performance was better at 30/18 sccm than at 52/35 sccm, although the former had lower stoichiometric requirements of feeding gases than the latter (Huang *et al.*, 2015; Huang *et al.*, 2016).

Table 1 summarizes the emission factors (EFs) of gas-phase and water-phase Total-PAHs and Total-BaP_{eq} for the anode and cathode and their sums under different operating flowrates or temperatures. The EF of anode gas-phase Total-PAHs increased with increasing flowrate (0.72±0.05, 1.51±0.01, 2.73±0.37, and 5.11±0.18 μg g-MEA^{-1} at 30/18, 52/35, 100/100, and 200/200 sccm, respectively, at 65°C) or temperature (1.51±0.01 and 1.59±0.07 μg g-MEA^{-1} at 65°C and 90°C respectively, at 52/35 sccm). A similar phenomenon was also observed for the EFs of cathode gas-phase Total-PAHs ((0.66±0.03)–(4.72±0.30) μg g-MEA^{-1}) and thus the sums of anode and cathode gas-phase Total-PAHs EFs (1.73±0.05, 3.02±0.09, 5.01±0.47, and 9.83±0.35 μg g-MEA^{-1} at 30/18, 52/35, 100/100, and 200/200 sccm, respectively, at 65°C and 3.19±0.13 μg g-MEA^{-1} at 90°C and 52/35 sccm). This result is attributed to the more mass of gas-phase PAHs desorbed from carbon material support at higher flowrate or temperature, and this PAH desorption behavior was more enhanced by increasing flowrate than by increasing temperature. Nevertheless, the EFs of anode and cathode gas-phase Total-PAHs were similar at 52/35 sccm regardless of difference in operating temperature, whereas the EFs of anode gas-phase Total-PAHs were higher than those of cathode ones. This result is possibly associated with the presence of the product (water) generated from the reaction 2 at cathode). The sums of anode and cathode gas-phase Total-PAHs EFs for a commercial E-TEK MEA in this study (3.02±0.09 μg g-MEA^{-1}) was lower than that of our previous study using a lab-prepared MEA (21.4±1.28 μg g-MEA^{-1}) (Huang *et al.*, 2016), primarily due to the differences in MEA weight and structure. However, it is not appropriate to directly

compare the PAH emission factors obtained in this study with those of fuel consumption or driving distance (mileage) based data reported in literature.

Increasing flowrate from 30/18 to 200/200 sccm at 65°C also increased the EFs of anode, cathode, and sum water-phase Total-PAHs ((1.15±0.02)–(1.34±0.02), (0.93±0.01)–(1.09±0.01), and (2.08±0.02)–(2.43±0.03) μg g-MEA^{-1}, respectively) (Table 1). However, the EFs of anode, cathode, and water-phase Total-PAHs were slightly greater at 65°C (1.17±0.04, 1.01±0.01, and 2.18±0.04 μg g-MEA^{-1}, respectively) than at 90°C (1.12±0.02, 0.91±0.01, and 2.03±0.02 μg g-MEA^{-1}, respectively). The difference between anode and cathode of water-phase Total-PAHs EFs was less than that of gas-phase Total-PAHs ones. The anode, cathode, and sum EFs were smaller for water-phase Total-PAHs than for gas-phase ones, except those at 30/18 sccm. The anode, cathode, and sum EFs of water-phase Total-BaP_{eq} ranged from (0.06±0.00)–(0.09±0.00), (0.02±0.00)–(0.03±0.03), and (0.08±0.00)–(0.12±0.00) μg g-MEA^{-1}, respectively, while those of gas-phase ones were (0.05±0.00)–(0.06±0.00), (0.03±0.00)–(0.06±0.03), and (0.08±0.00)–(0.12±0.00) μg g-MEA^{-1}, respectively. Accordingly, it is suggested that the fuel cell should be operated at anode/cathode flowrates of 52/35 (or 30/18) and 65°C to reduce the emissions of gas- and water-phase PAHs and achieve appropriate MEA's performance.

It is known that at equilibrium, the air-water partition coefficient (K_{AW}) of a PAH species is equal to H/RT, where H, R, and T are Henry's constant, gas constant, and absolute temperature, respectively (Shiu and Mackay, 1997; Bamford *et al.*, 1999). PAHs usually show a trend of diminishing H or K_{AW} with increasing molecular mass at constant temperature (Shiu and Mackay, 1997); however, the K_{AW} increases when temperature rises (Bamford *et al.*, 1999). In this study, the fuel cell system might possibly reach steady-state in the operation at fixed flowrate and temperature, but it was not the case of equilibrium. Therefore, it is not appropriate to use our gas- and

400 water-phase PAH data for K_{AW} calculation.

401

402 ## CONCLUSIONS

403 In this study, at anode/cathode flowrates of 52/35 sccm, the concentrations of
404 PAHs in anode and cathode emission gas ranged from not detectable (ND) (BeP) to
405 2.961±0.005 (Nap) and ND (BeP) to 4.115±0.005 (Nap) μg Nm^{-3}. Roughly, the
406 concentrations of individual gas- and water-phase PAHs decreased when feeding gas
407 flowrate increased, and the anode PAH concentrations were lower than the cathode
408 ones at 65°C. At 52/35 sccm, the concentrations of gas-phase PAHs were similar at
409 both 65°C and 90°C, while the water-phase PAH concentrations were greater at 65°C
410 than at 90°C. Similar concentration profiles were observed for anode, cathode, or
411 anode vs. cathode gas-phase PAHs under various flowrates or temperatures; however,
412 those for water-phase PAHs were partially different, and the gas- and water-phase
413 PAHs had different concentration profiles.

414 The concentrations of molecular-weight (MW) classified PAHs in anode and
415 cathode emission gases varied with the order LMM- > HMM- > MMM-PAHs under
416 different flowrates (except 18 sccm) or temperatures, and the gas-phase Total-PAHs or
417 Total-BaP_{eq} concentration decreased with the increase of flowrate (except 30/18 sccm).
418 At 52/35 sccm, the concentrations of gas-phase LMW-, MMW-, and HMW-PAHs at
419 65°C were similar to those at 90°C; therefore, the gas-phase Total-PAHs or
420 Total-BaP_{eq} concentrations were also similar at both temperatures (Total-PAHs:
421 8.892±0.079 and 13.18±0.792 μg Nm^{-3} for anode and cathode, respectively;
422 Total-BaP_{eq}: 0.365±0.001 and 0.546±0.004 μg Nm^{-3} for anode and cathode,
423 respectively, at 65°C). The concentrations of water-phase Total-PAHs were higher at
424 65°C (7.940±0.149 μg L^{-1} and 32.09±0.185 μg L^{-1} for anode and cathode effluents,
425 respectively) than at 90°C. The Total-BaP_{eq} concentration in anode and cathode

effluents were 0.440±0.003 and 0.893±0.005 μg L^{-1}, respectively, at 65°C.

The performance of MEA decreased with increasing flowrate or temperature. The EF sum (anode + cathode) for gas- or water-phase Total-PAHs increased with increasing flowrate. This tendency is also true for gas-phase Total-PAHs EFs but not for water-phase Total-PAHs EFs when raising temperature from 65°C to 90°C. At 65°C and 52/35 sccm, the EF sums of water-phase Total-PAHs and Total-BaP_{eq} were 2.18±0.04 and 0.09±0.00 μg g-MEA^{-1}, respectively, smaller than those of gas-phase ones (3.02±0.09 and 0.12±0.00 μg g-MEA^{-1}, respectively).

ACKNOWLEDGEMENT

The authors would like to thank the Ministry of Science and Technology, Taiwan, R.O.C. for financially supporting this research under Grant Nos. MOST 96-2211-E-020-011-MY2 and 106-2221-E-020-003-MY3.

REFERENCES

Bamford, H.A., Poster, D.L. and Baker, J.E. (1999). Temperature Dependence OF Henry's Law Constants of Thirteen Polycyclic Aromatic Hydrocarbons Between 4°C and 31°C. *Environ. Toxicol. Chem.* 18(9): 1905–1912.

ER Wiki accessible 10/07/2017, Polycyclic Aromatic Hydrocarbons (PAHs), http://www.environmentalrestoration.wiki/index.php?title=Polycyclic_Aromatic_Hydrocarbons_(PAHs).

Fan, Z.L., Chen, X.C., Lui, K.H., Ho, S.S.H., Cao, J.J., Lee, S.C., Huang, H. and Ho, K.F. (2017). Relationships between Outdoor and Personal Exposure of Carbonaceous Species and Polycyclic Aromatic Hydrocarbons (PAHs) in Fine Particulate Matter (PM2.5) at Hong Kong. *Aerosol Air Qual. Res.* 17: 666–679.

Huang, K.L., Lai, Y.C. and Tsai, C.H. (2006). Effects of Sputtering Parameters on the

Performance of Electrodes Fabricated for Proton Exchange Membrane Fuel Cells. *J. Power Sources* 156: 224–231.

Huang, K.L., Tsai, T.H., Tsai, J.H., Chen, S.J., and Lee, W.J. (2015). Emission of PAHs from a Single Hydrogen-Oxygen PEM Fuel Cell: In relation to Fuel Cell Carbon Materials. *Aerosol Air Qual. Res.* 15: 2654–2667.

Huang, K.L., Wu, M.S., Tsai, J.H., Lin, D.Y., Chen, S.J. and Lee, W.J. (2016). Effect of Operating Conditions on PAHs Emission from a Single H_2-O_2 PEM Fuel Cell. *Aerosol Air Qual. Res.* 16: 2186–2197.

Kah, M., Zhang, X., Jonker, M.T. and Hofmann, T. (2011) Measuring and Modeling Adsorption of PAHs to Carbon Nanotubes over a Six Order of Magnitude Wide Concentration Range. *Environ. Sci. Technol.* 45: 6011–6017.

Kavouras, I.G., DuBois, D.W., Nikolich, G. and Etyemezian, V. (2015). Monitoring, Source Identification and Health Risks of Air Toxics in Albuquerque, New Mexico, U.S.A. *Aerosol Air Qual. Res.* 15: 1160–1167.

Lai, Y.C., Huang, K.L., Tsai, C.H., Lee, W.J. and Chen, Y.L. (2012). Sputtered Pt loadings of membrane electrode assemblies in proton exchange membrane fuel cells. *Int. J. Energy Res.* 32(8): 918–927.

Lai, Y.C., Tsai, C.H., Chen, Y.L. and Chang-Chien, G.P. (2017). Distribution and Sources of Atmospheric Polycyclic Aromatic Hydrocarbons at an Industrial Region in Kaohsiung, Taiwan. *Aerosol Air Qual. Res.* 17: 776–787.

Lee, J.J., Huang, K.L., Yu, Y.Y. and Yang, S.C. (2004). Laboratory Retention of Vapor-phase PAHs Using XAD Adsorbents. *Atmos. Environ.* 38(36): 6185–6193.

Lee, D. and Lee, D.G. (2016). Carbon Composite Bipolar Plate for High-Temperature Proton Exchange Membrane Fuel Cells (HT-PEMFCs). *J. Power Sources* 327: 119–126.

Li, Y.Y., Yang, L.X., Chen, X.F., Gao, Y., Jiang, P., Zhang, J.M., Yu, H. and Wang,

W.X. (2017). $PM_{2.5}$-Bound PAHs in Indoor and Outdoor of Hotels in Urban and Suburban of Jinan, China: Concentrations, Sources, and Health Risk Impacts. *Aerosol Air Qual. Res.* 17: 2463–2473.

Ma, X and Uddin S. (2013). Desorption of 1,3,5-Trichlorobenzene from Multi-Walled Carbon Nanotubes: Impact of Solution Chemistry and Surface Chemistry. *Nanomaterials* 3: 289–302.

Moninot, G. (2010). Where are the PAHs in the Carbon Black? Available at www.iom3.org/fileproxy/331784 (accessed Aug. 2015)

Mwangi, J.K., Lee, W.J., Tsai, J.H. and Wu, T.S. (2015). Emission Reductions of Nitrogen Oxides, Particulate Matter and Polycyclic Aromatic Hydrocarbons by Using Microalgae Biodiesel, Butanol and Water in Diesel Engine. *Aerosol Air Qual. Res.* 15: 1160–1167.

Nisbet, C. and LaGoy, P. (1992). Toxic Equivalency Factors (TEFs) for Polycyclic Aromatic Hydrocarbons (PAHs). *Regul. Toxicol. Pharmacol.* 16: 290–300.

Pongpiachan, S. (2016). Incremental Lifetime Cancer Risk of PM2.5 Bound Polycyclic Aromatic Hydrocarbons (PAHs) Before and After the Wildland Fire Episode. *Aerosol Air Qual. Res.* 16: 2907–2919.

Reshetenko, T., Serov A., Artyushkova K., Matanovic I., Stariha S. and Atanassov, P. (2016). Tolerance of Non-Platinum Group Metals Cathodes Proton Exchange Membrane Fuel Cells to Air Contaminants. *J. Power Sources* 324: 556–571.

Scofield, M.E., Liu, H. and Wong, S.S. (2015). A Concise Guide to Sustainable PEMFCs: Recent Advances in Improving Both Oxygen Reduction Catalysts and Proton Exchange Membranes. *Chem. Soc. Rev.* 44: 5836–5860.

Shiu, W.Y. and Mackay, D. (1997). Henry's Law Constants of Selected Aromatic Hydrocarbons, Alcohols, and Ketones. *J. Chem. Eng. Data* 42: 27–30.

Stogiannidis, E. and Laane, R. (2015). Source Characterization of Polycyclic

Aromatic Hydrocarbons by Using Their Molecular Indices: An Overview of Possibilities, Vol. 234, In Whitacre, D.M. (Ed.) Reviews of Environmental Contamination and Toxicology, Springer International Publishing, Switzerland, p. 56–72.

Tenson, T.J. and Baby, R. (2017). Recent Advances in Proton Exchange Membrane Fuel Cells: A Review. *IJARSET* 4(SI 6): 34–40.

Tiwari, M., Sahu, S.K. and Pandit, G.G. (2015). Inhalation Risk Assessment of PAH Exposure Due to Combustion Aerosols Generated from Household Fuels. *Aerosol Air Qual. Res.* 15: 582–590.

Tran, P.D., Morozan, A., Archambault, S., Heidkamp, J., Chenevier, P., Dau, H., Fontecave, M., Martinent, A., Jousselme B. and Artero, V. (2015). A Noble Metal-free Proton-exchange Membrane Fuel Cell Based on Bio-inspired Molecular Catalysts. *Chem. Sci.* 6: 2050–2053.

Wang, X., Zhang, H., Zhang, J., Xu, H., Zhu, X.B., Chen, J. and Yi, B.L. (2006). A Bi-functional Micro-porous Layer with Composite Carbon Black for PEM Fuel Cells. *J. Power Sources* 162: 474–479.

Zhang, J.Q., Zhan, C.L., Liu, H.X., Liu, T., Yao, R.H. Hu, T.P., Xiao, W.S., Xing, X.L., Xu, H.M. and Cao, J.J. (2016). Characterization of Polycyclic Aromatic Hydrocarbons (PAHs), Iron and Black Carbon within Street Dust from a Steel Industrial City, Central China. *Aerosol Air Qual. Res.* 16: 2452–2461.

Zhang, C.L., Shen, X.C., Pan, Y.B. and Peng, Z.M. (2017). A review of Pt-based Electrocatalysts for Oxygen Reduction Reaction. Front. Energy 11(3): 268–285.

Zeis, R. (2015). Materials and Characterization Techniques for High-temperature Polymer Electrolyte Membrane Fuel Cells. *Beilstein J. Nanotechnol.* 6: 68–83.

529 **Table 1**. Emission factors (EFs) of gas-phase and water-phase Total-PAHs and
530 Total-BaP_{eq} for the anodes (A), cathodes (C), and sums (A + C) under different
531 operating flowrates or temperatures.

A/C (sccm)	T (^{o}C)	Total-PAHs EFs (μg g-MEA^{-1})			Total-BaP_{eq} EFs (μg g-MEA^{-1})		
Gas-phase		A	C	Sum	A	C	Sum
30/18	65	0.72±0.05	0.66±0.03	1.37±0.05	0.06±0.00	0.04±0.00	0.10±0.00
52/35	65	1.51±0.01	1.51±0.09	3.02±0.09	0.06±0.00	0.06±0.00	0.12±0.00
100/100	65	2.73±0.37	2.28±0.29	5.01±0.47	0.05±0.00	0.05±0.00	0.10±0.00
200/200	65	5.11±0.18	4.72±0.30	9.83±0.35	0.05±0.00	0.03±0.00	0.08±0.00
52/35	90	1.59±0.07	1.60±0.11	3.19±0.13	0.06±0.00	0.06±0.00	0.12±0.00
Water-phase		A	C	Sum	A	C	Sum
30/18	65	1.15±0.02	0.93±0.01	2.08±0.02	0.09±0.00	0.03±0.00	0.12±0.00
52/35	65	1.17±0.04	1.01±0.01	2.18±0.04	0.06±0.00	0.03±0.00	0.09±0.00
100/100	65	1.21±0.03	1.03±0.02	2.24±0.04	0.06±0.00	0.02±0.00	0.08±0.00
200/200	65	1.34±0.02	1.09±0.01	2.43±0.03	0.06±0.00	0.03±0.00	0.09±0.00
52/35	90	1.12±0.02	0.91±0.01	2.03±0.02	0.07±0.00	0.02±0.00	0.09±0.00

532
533

Figure Captions

Fig. 1. The scheme of single PEMFC for PAH emission tests (W: water-phase PAHs collector, X: gas-phase PAHs collector (cartridge), Y: flow meter, and Z: pump).

Fig. 2. Characteristic profiles of gas-phase PAHs emitted at different PEMFC anode/cathode flowrates (65^{o}C): (a) 52/35, (b) 30/18, (c) 100/100, and (d) 200/200 sccm (n = 3).

Fig. 3. Characteristic profiles of water-phase PAHs emitted at different PEMFC anode/cathode flowrates (65^{o}C): (a) 52/35, (b) 30/18, (c) 100/100, and (d) 200/200 sccm (n = 3).

Fig. 4. Characteristic profiles of PAHs emitted at 90^{o}C ((a) gas-phase (G) and (b) water-phase (W)) (anode/ cathode = 52/35 sccm) (n = 3).

Fig. 5. Comparison of PAHs concentration fraction profiles (normalized to Total-PAHs concentration at different PEMFC anode/cathode flowrates (52/35, 30/18, 100/100, and 200/200 sccm) and temperature (65^{o}C and 90^{o}C) (n = 3). (a) anode (A) gas-phase (G), (b) cathode (C) gas-phase, (c) anode water-phase (W), and (d) cathode water-phase.

Fig. 6. Concentrations of gas-phase LMW-, MMW-, HMW-, and Total-PAHs and Total-BaP_{eq} at different flowrates ((a) anode and (b) cathode) and temperatures (c) (n = 3).

Fig. 7. Concentrations of water-phase LMW-, MMW-, HMW-, and Total-PAHs and Total-BaP_{eq} at different flowrates ((a) anode and (b) cathode) and temperatures (c) (n = 3).

Fig. 8. Polarization (current-potential) curves under different operating conditions for the PEMFC.

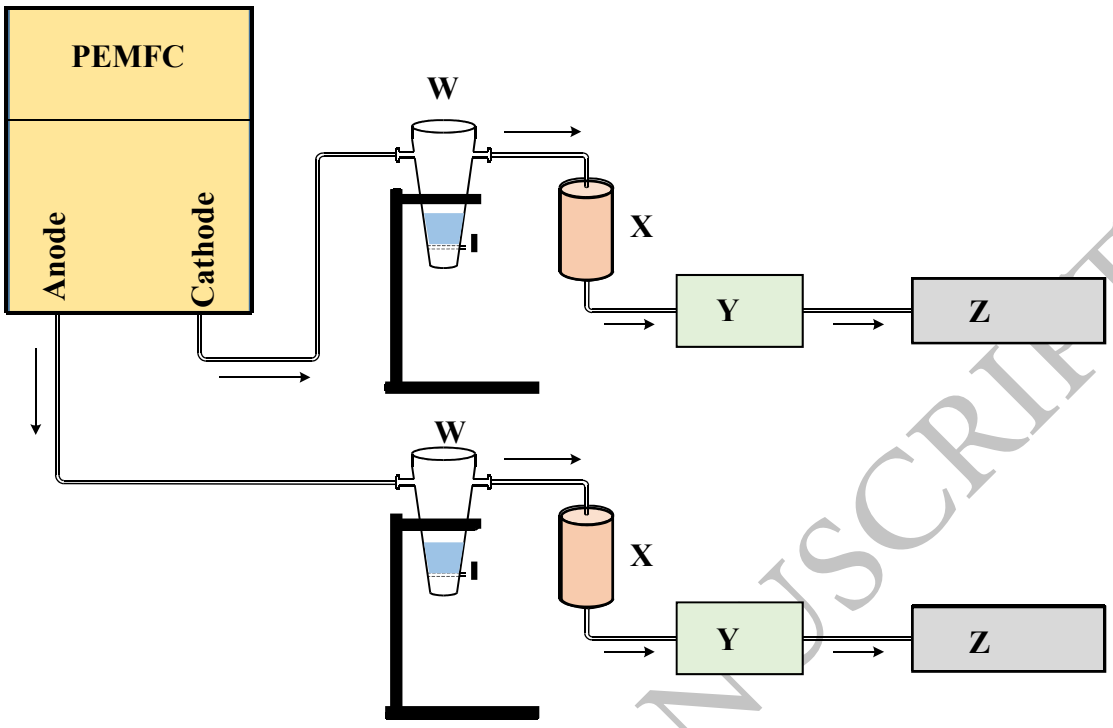

Fig. 1. The scheme of single PEMFC for PAH emission tests (W: water-phase PAHs collector, X: gas-phase PAHs collector (cartridge), Y: flow meter, and Z: pump).

580

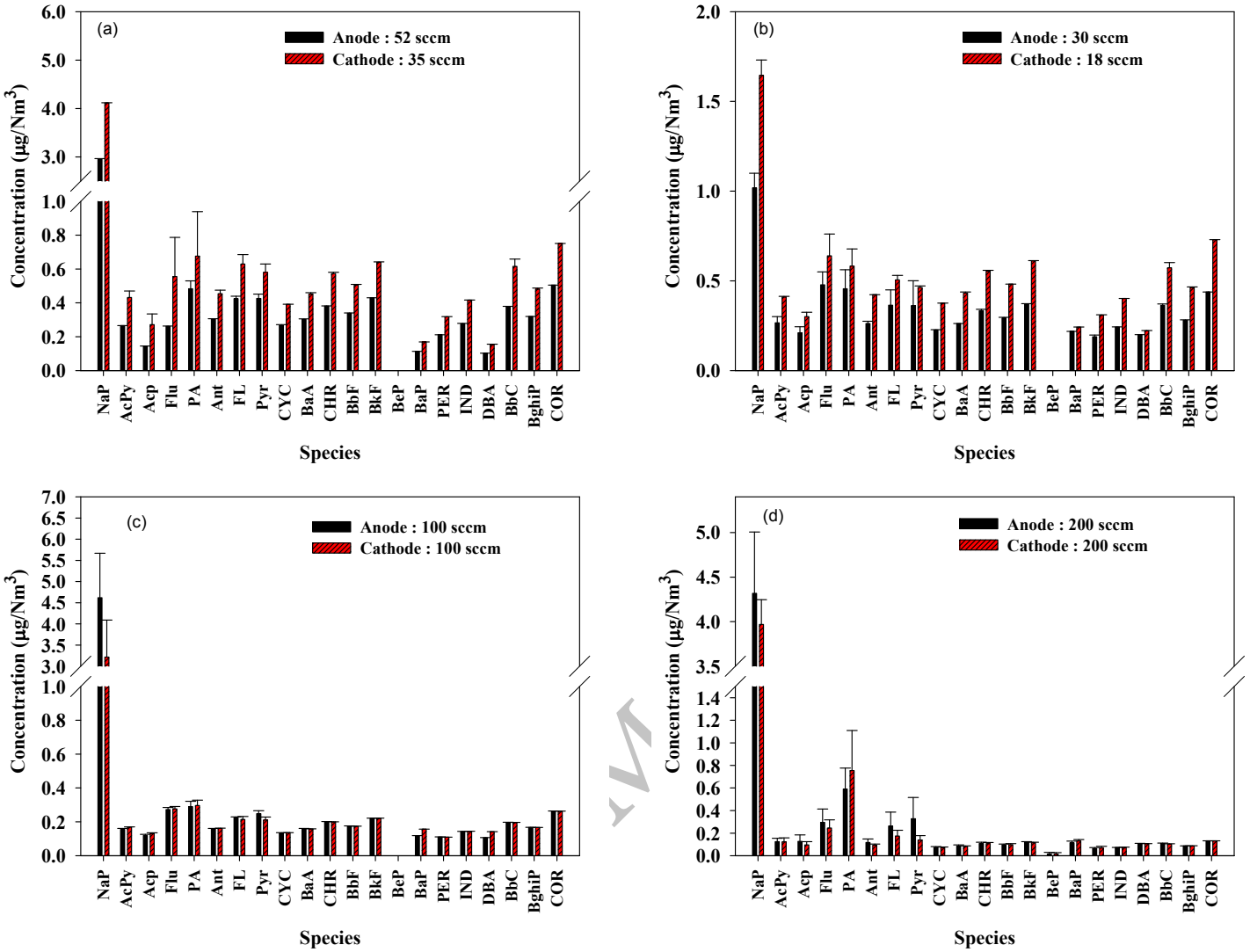

581 **Fig. 2.** Characteristic profiles of gas-phase PAHs emitted at different PEMFC
582 anode/cathode flowrates (65°C): (a) 52/35, (b) 30/18, (c) 100/100, and (d) 200/200
583 sccm (n = 3).
584

585

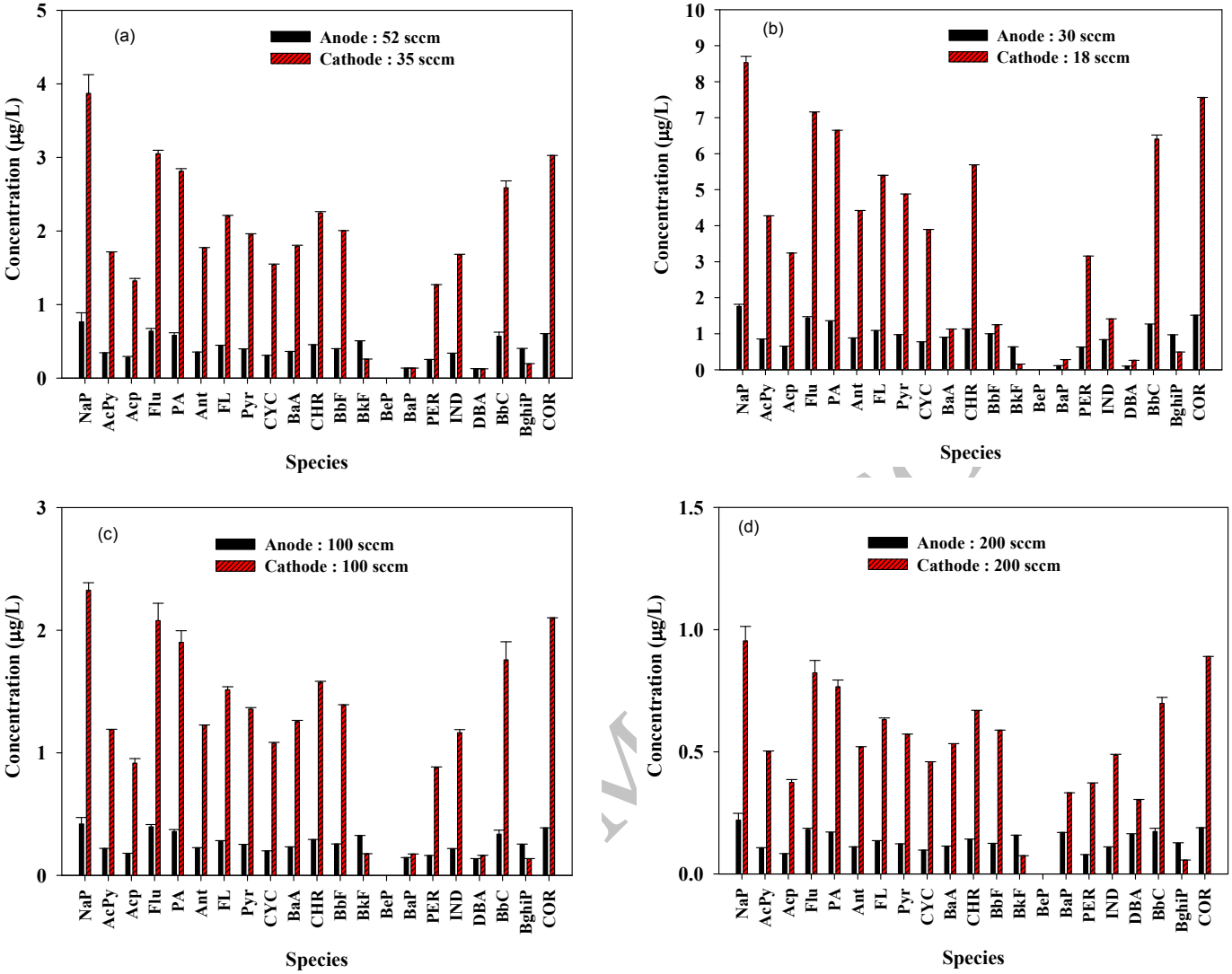

586 **Fig. 3.** Characteristic profiles of water-phase PAHs emitted at different PEMFC
587 anode/cathode flowrates (65°C): (a) 52/35, (b) 30/18, (c) 100/100, and (d) 200/200
588 sccm (n = 3).
589
590

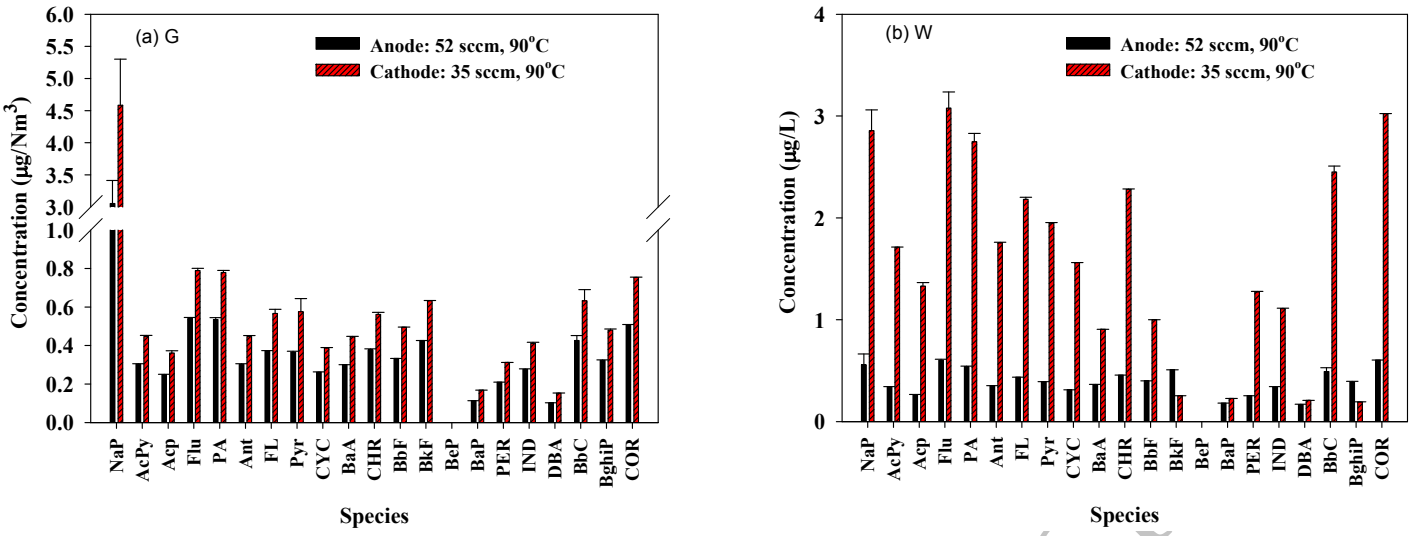

591 **Fig. 4.** Characteristic profiles of PAHs emitted at 90°C ((a) gas-phase (G) and (b)
592 water-phase (W)) (anode/ cathode = 52/35 sccm) (n = 3).
593
594

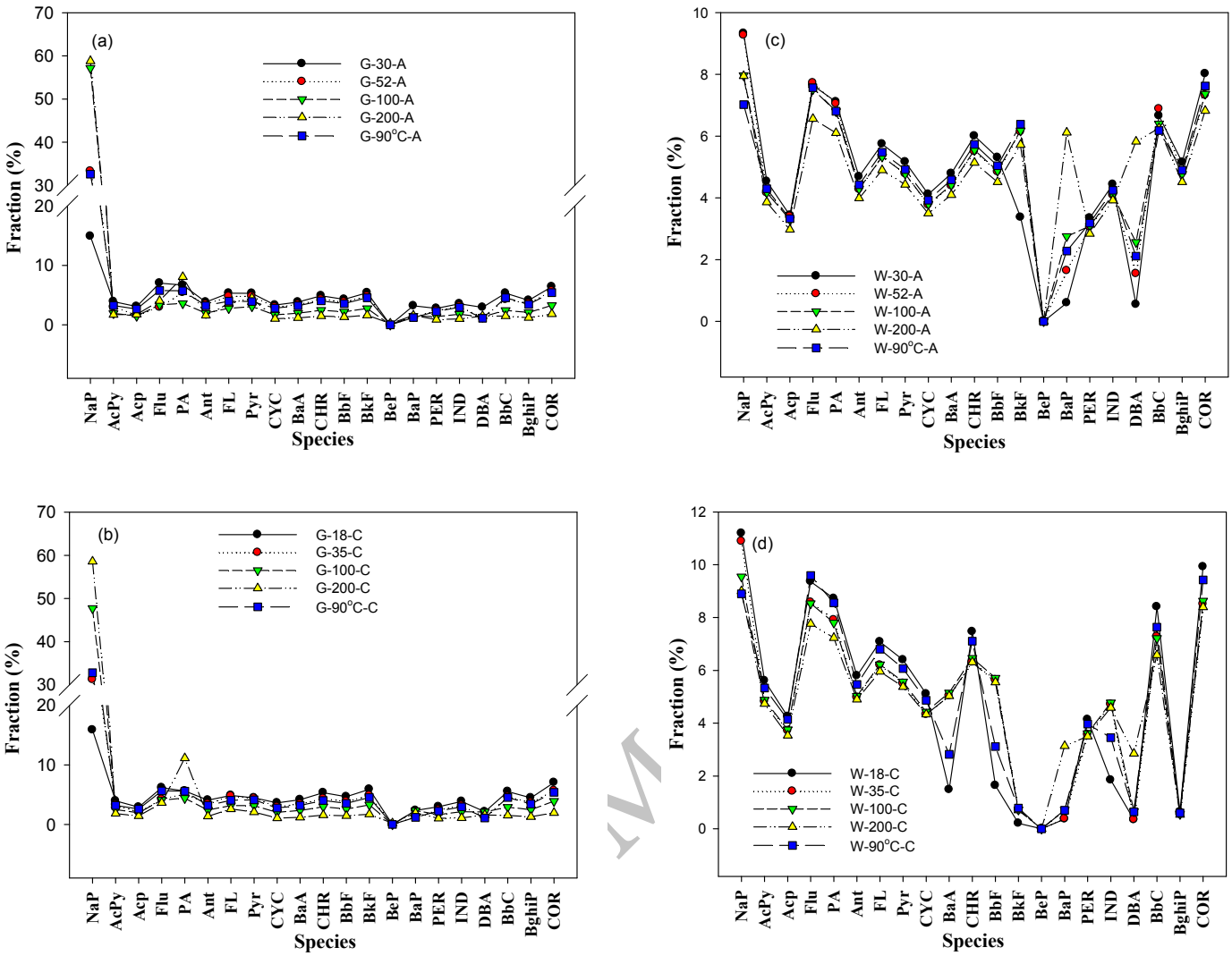

595 **Fig. 5.** Comparison of PAHs concentration fraction profiles (normalized to
596 Total-PAHs concentration at different PEMFC anode/cathode flowrates (52/35, 30/18,
597 100/100, and 200/200 sccm) and temperature (65°C and 90°C) (n = 3). (a) anode (A)
598 gas-phase (G), (b) cathode (C) gas-phase, (c) anode water-phase (W), and (d) cathode
599 water-phase.
600
601

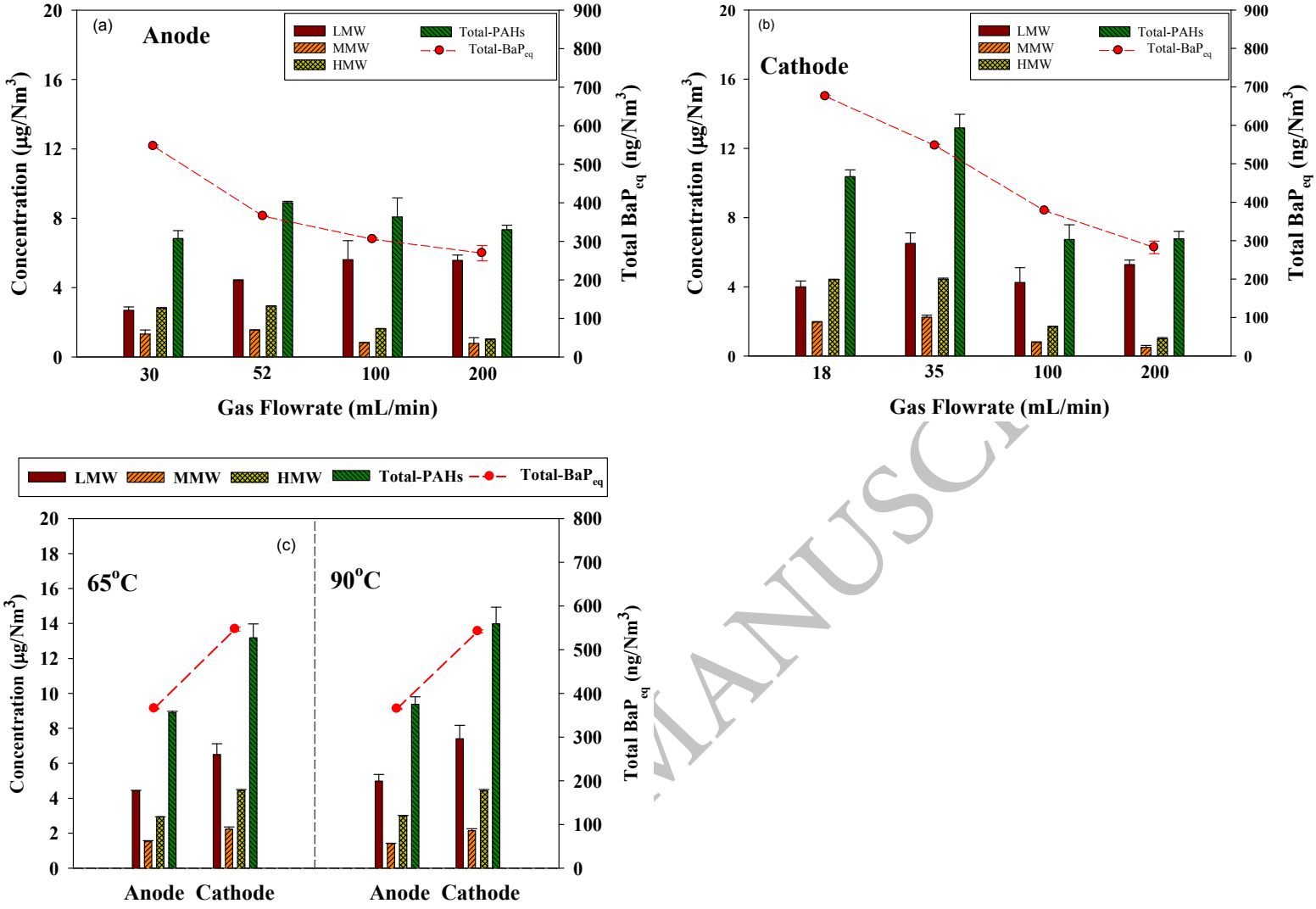

602 **Fig. 6.** Concentrations of gas-phase LMW-, MMW-, HMW-, and Total-PAHs and
603 Total-BaP$_{eq}$ at different flowrates ((a) anode and (b) cathode) and temperatures (c) (n
604 = 3).
605
606

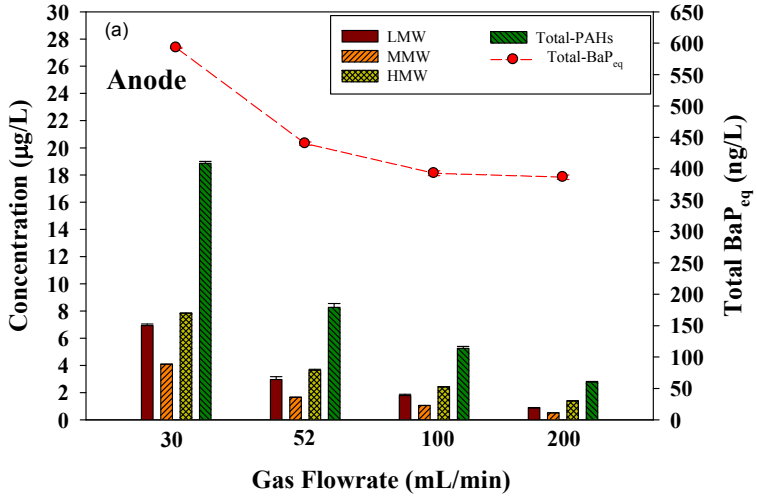

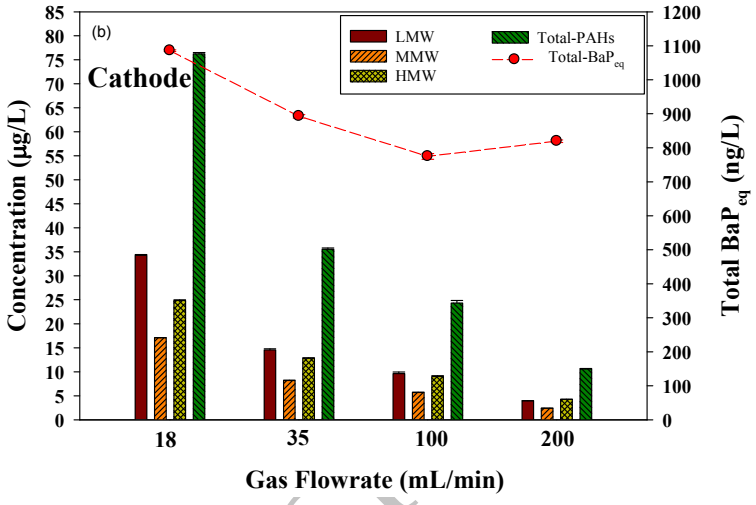

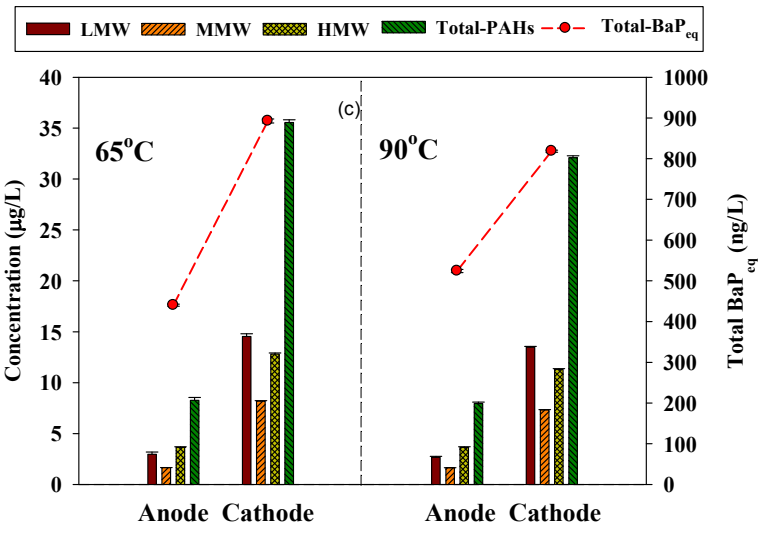

607 **Fig. 7.** Concentrations of water-phase LMW-, MMW-, HMW-, and Total-PAHs and
608 Total-BaP_{eq} at different flowrates ((a) anode and (b) cathode) and temperatures (c) (n
609 = 3).
610
611

612

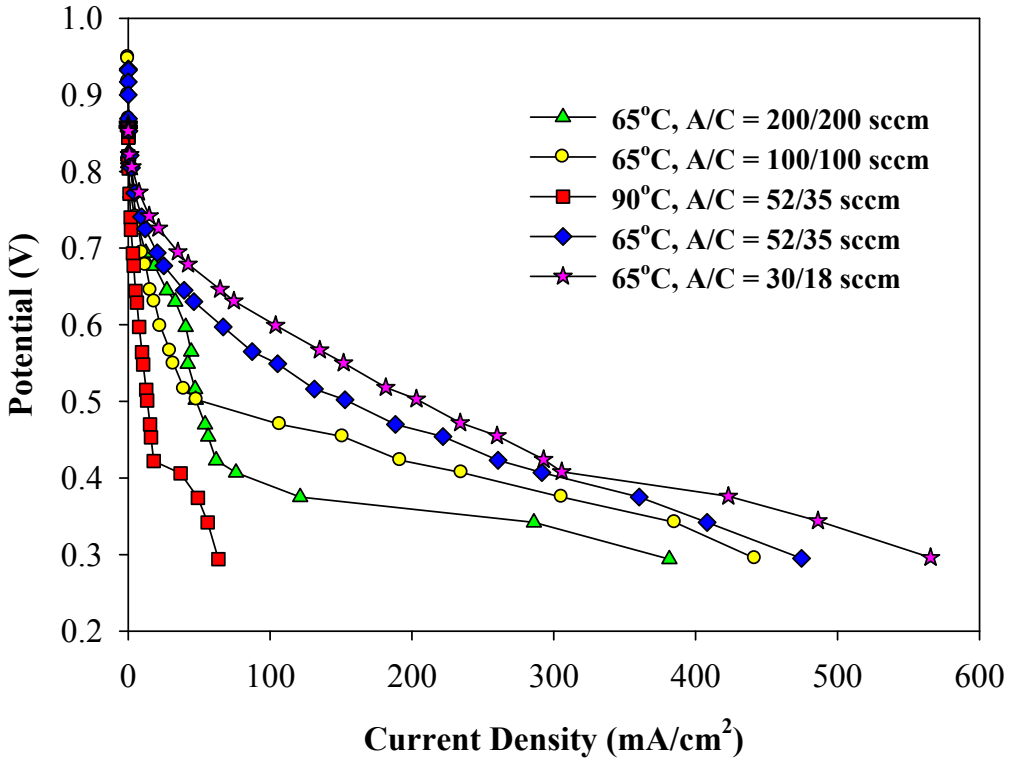

613

614 **Fig. 8.** Polarization (current-potential) curves under different operating conditions for
615 the PEMFC.

616